Registration of Total Hip Replacement Implants from Subjects Imaged with 1.5 and 3 Tesla MRI Scanners Using Mavric

Theodore Lawrence DeGroot
Marquette University

REGISTRATION OF TOTAL HIP REPLACEMENT IMPLANTS FROM SUBJECTS IMAGED WITH 1.5 AND 3 TESLA MRI SCANNERS USING MAVRIC

by

Theodore DeGroot B.S.

A Thesis submitted to the Faculty of the Graduate School, Marquette University,
in Partial Fulfillment of the Requirements for
the Degree of Master of Science

Milwaukee, Wisconsin

December 2019

ABSTRACT
REGISTRATION OF TOTAL HIP REPLACEMENT IMPLANTS FROM SUBJECTS IMAGED WITH 1.5 AND 3 TESLA MRI SCANNERS USING MAVRIC

Theodore DeGroot, B.S. Marquette University, 2019

Introduction: Total hip arthroplasty (THA) is a common treatment to correct arthritis and necrosis ailing the hip joint. An array of diseases can occur in response to the presence and wear of the implant. MRI is an imaging modality that can assess and diagnosis the diseases ailing the periprosthetic tissues, however images of a metal implants are susceptible to artifacts. Aim 1 of this study was to register the THAs imaged at 3T to 1.5T images; Aim 2 was to validate that metal susceptibility artifacts increase with field strength.

Methods: 21 subjects with a total of 29 hip prosthetics that had coronal MAVRIC SL scans at 1.5T of their hips were recruited to be rescanned at 3T. MAVRIC SL is GE's metal artifact reducing acquisition technology. The prosthetics imaged at 1.5T and 3T were then registered together. The acetabular and femoral component had to be registered independently since they are separate rigid bodies. The acetabular was registered by finding the registration transformation of a bone fixed to the component, then applying this transform to the 3T acetabular volume. The femoral components were registered by taking three anatomical landmarks and registering them together using a least-squares fitting of 3-D points algorithm. Lastly, the two 3T components were combined and then registered to the 1.5T prosthetic. The size of the volume of the of 1.5T and 3T images were compared.

Results: Of the 29 hips scanned, 25 were viable for this study. The percent alignment of the 1.5T and 3T acetabular volumes had a mean = 90.03%, SD = 8.64%. For the femoral component the alignment had a mean = 67.89% and SD = 14.74. The total alignment had a mean = 77.64% and SD = 12.64%. The 3T artifact volumes were 7.93% and 5.49% smaller than the 1.5T volumes for the acetabular and femoral components respectively.

Conclusion: While the acetabular component registration was successful, work still needs to be done for the femoral registration. The size of the artifact was larger at 1.5T than 3T, this was not expected and is a result of user error when tracing the two components.

Table of Contents

1 Introduction:

1.1 Hip Arthroplasty: Details of procedure

There are several reasons why patients may undergo a total hip arthroplasty; osteoarthritis, rheumatoid arthritis, post-traumatic arthritis, avascular necrosis, and a childhood hip disease [1]. Osteoarthritis is an age related disease, often associated with a family history of arthritis, where the cartilage between the acetabulum (hip socket) and femoral head (hip ball) deteriorates. When this happens the two bones begin to rub against one another causing stiffness and pain. Rheumatoid arthritis is a form of arthritis that is presented by inflammation or thickening of the synovial membrane. Post-traumatic arthritis is caused by a traumatic event like those experienced in car accidents, falls, or sports. These traumatic incidences may result in damage to the bone and cartilage, leading to complications similar to other arthritis diseases. Avascular necrosis is caused by an injury that results in the limitation of blood flow to the femoral head. This will cause the surface of the bone to deteriorate, and arthritis will also occur. Less common, a childhood hip disease can necessitate HA. These diseases occur when a child's hip does not develop properly. While it might be treated during childhood, HA can be necessary later in life if arthritis occurs.

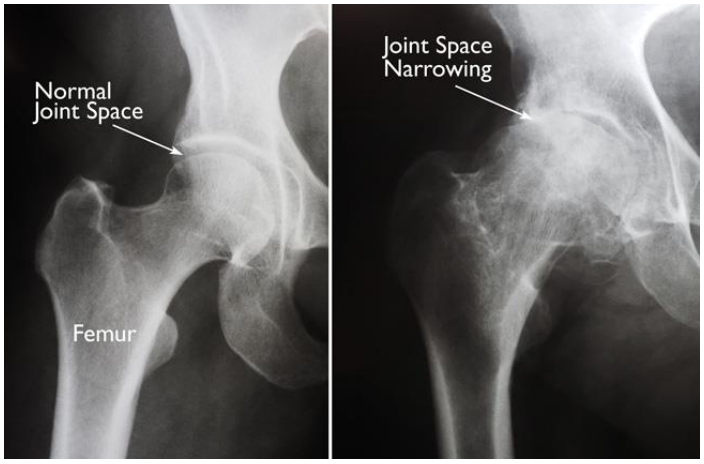

Figure 1. Cartilage degradation presented by a narrowing of hip joint space. It is seen that the left hip (healthy) has normal spacing throughout the joint space, while the diseased hip exhibits a narrowed joint space indicating cartilage degradation. [1]

The above diseases can progress to the level where surgical intervention is required. THA may be suggested by the physician if pain from the hip dysfunction limits normal daily activity, cause pain while at rest, mobility of the hip is limited, or if pain relief isn't achieved through physical therapy or anti-inflammatory drugs. Before the surgery an orthopedic surgeon will evaluate the patient's status from multiple fronts. First the patient's medical history will be examined; including family history, pain levels, and performance of daily activities. A physical examination will be conducted to determine the strength and mobility of the hip joint. The imaging standard for assessment of the damage and deformation is X-ray. One way of assessing cartilage damage with X-ray is to examine joint spacing. A healthy joint will exhibit a consistent spacing throughout the socket, an arthritic hip will have a narrowing of this hip joint (figure 1.). An MRI can be ordered to further assess soft tissue or bone damage [1].

If it is determined that bone and/or cartilage damage is severe enough a patient will undergo a total hip replacement. The femoral head of the bone is removed and the femur is hollowed out. The femoral component of the implant has two parts, the stem and the head. The stem is inserted and sometimes cemented into the hollowed out portion of the femur. The head section is either ceramic or metal. The damaged cartilage and part of the acetabulum is removed and a metal socket is inserted. Between the head and the acetabular component there is a plastic, ceramic, or metal spacer. Following surgery, the patient will be advised to keep weight off the hip for 3 to 6 weeks, then resume normal light activity. Immediate complications from the surgery may include infection, blood clots, leg-length inequality, or joint dislocation. These complications can be limited by taking antibiotics to prevent infections, blood thinners to reduce chances of clotting, and avoiding situations where a fall may cause damage to the new hip joint [1]

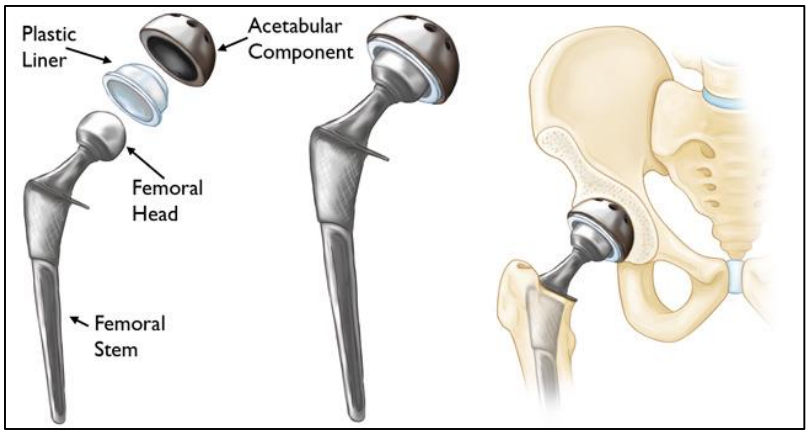

Figure 2. Three components common to total hip arthroplasty, and their placement in the hip joint. [1]

1.2 Hip Arthroplasty: Long Term Complications

Progressive THA failure is caused in part to particles created by the wear and corrosion of implant devices. These particles can trigger an inflammatory response that may result in adverse local tissue reactions (ALTR) [2], such as aseptic lymphocytic vasculitis-associated lesions (ALVAL) [3], metallosis [4], and pseudotumors [5]. The synovial membrane (a soft tissue envelope which encapsulates a joint) dysfunction has been shown to correlate with ALTR severity [6]. Osteolysis is another possible complication of THA where bone is resorbed leading to prosthetic loosening. Currently these diseases are diagnosed with projection imaging modalities due to insufficient training for diagnosis using MRI, and the greater cost of a scan. Evidence of dysfunction may only be visible on radiographs if the disease has progressed to a severe state. A sufficient cohort of subjects who have undergone THA would provide a training set that could allow for deep learning segmentation and quantification of synovial abnormalities, giving physicians the capability of earlier diagnosis.

1.2.1 Aseptic Lymphocytic Vasculitis-Associated Lesions

ALVAL, first described in 2005, consists of an array of diseases that are associated with HA [6]. Typically a precursor to lymphoid neogenesis, ALVAL is related to chronic inflammatory diseases, and can result in necrosis and hip failure. ALVAL commonly is associated with patients who have undergone a metal on metal THA (MoM). This disease can result in pain, swelling, nerve palsy, dislocation, and periprosthetic fracture [7]. While studies examined by Yannay et al. have shown an occurrence of 14-36%, no demographic predilection has been shown.

Radiographs have been shown to work for patient surveillance and investigation of symptomatic and failing prostheses [8]. Typically, failure of a prosthetic will be exhibited by resorption of the femoral neck and avascular necrosis. This modality has been shown to identify medial calcar resorption, which anecdotal evidence suggests might have a correlation to ALVAL. However, this modality is limited in its assessment of soft tissue damage due to radiography's low contrast capabilities for soft tissues.

A surgical investigation might be ordered if there is limited mobility, high pain, or the radiographs suggest failure. Surgical investigation of a failed hip replacement can show that the cavity that is related to the joint is lined by a thick, pale, and avascular fibrinous membrane usually containing a milky septic fluid [8]. While visible metal particles are uncommon, soft tissue necrosis of the gluteal tendons and osteonecrosis of the proximal femur has been noted in hip failure. Structures of these failed hips appear pale or white and devitalized. Histology of the tissue is also a way to determine the severity of ALVAL. Campbell et al. proposed a grading system for assessing classifying ALVAL [9].

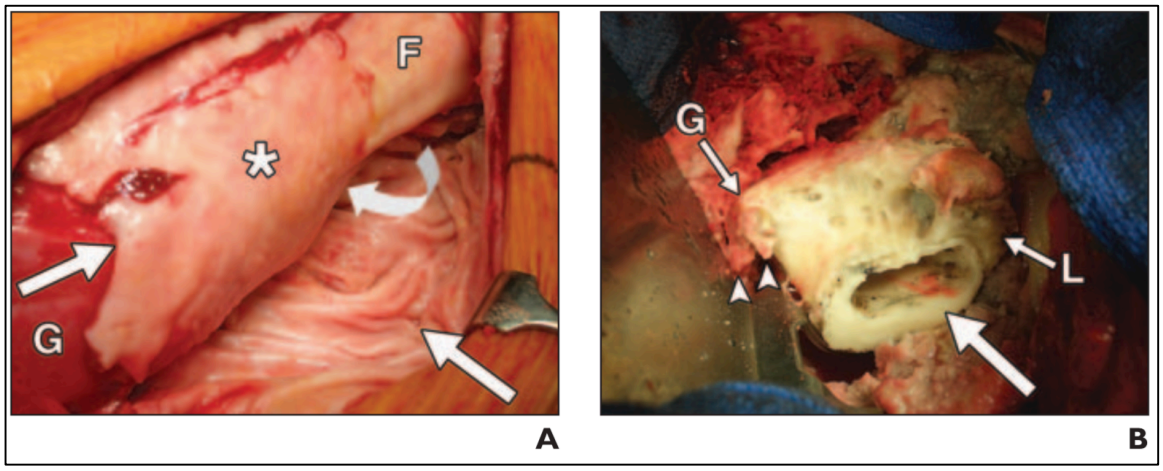

Figure 3. A: A 72-year-old woman exhibiting ALVAL by a typical large periprosthetic fluid filled cavity, and a large thick layer of fibrinous tissue (straight arrow). **B:** A 69-year-old male with more severe ALVAL. Removed prosthetic shows soft tissue and bone necrosis. The proximal femur is devitalized at the greater (G) and lesser (L) trochanter. [8]

MRI is limited in its assessment of ALVAL and other diseases around metal implants due to the prosthetic causing artifacts in adjacent soft tissues and bone. Methods to reduce metal artifacts include using thinner sections or reducing voxel size, increasing frequency encoded strength, using spin-echo or fast spin-echo sequences rather than gradient echo, using short Tau inversion recovery, using broader bandwidth, imaging with scanners that have a lower magnetic field strength, and imaging the prosthesis with its long axis longitudinal to the static field [6]. Imaging a prosthetic with a larger metal bearing causes even greater metal artifacts in the surrounding tissues. ALVAL will be have a stronger fluid signal due to the aseptic fluid associated with the disease.

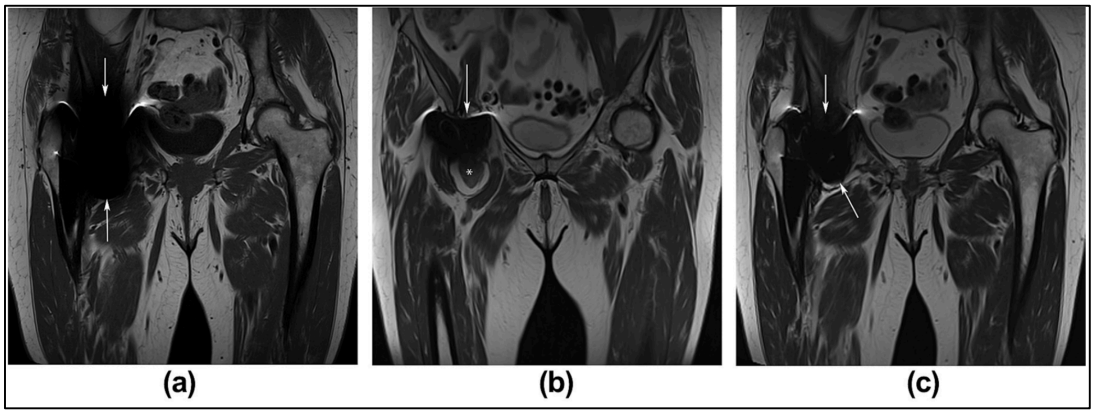

Figure 4. A: T_2, **B:** FSE, **C:** MARS images of a THA in a patient complaining of pain. Low T_1 and intermediate T_2 signal were seen in these images, as well as a soft tissue mass anterior to the prosthesis near iliopsoas tendon. Following a surgical biopsy, this mass was histologically proven to be ALVAL. [6]

Anderson et al. conducted a study where they examined 73 HA across 59 patients imaged using Siemans MAR technology [10]. They had three observers look over the patients and used a scoring system they designed to assess agreement in diagnosis across patients. The observers were made of three musculoskeletal radiologists, two more experienced with diagnosing MoM diseases, and one unfamiliar with these diagnoses. The scores were A: normal, B: infection, C1: mild MoM disease, C2: moderate MoM disease, and C3: severe MoM disease. Using kappa correlation statistics it was determined that the two experienced radiologists had the highest rate of agreement wit $\boldsymbol{\kappa}$ = 0.78, between the two experienced and the one inexperienced observer the agreement was still substantial with $\boldsymbol{\kappa}$ = 0.69 and $\boldsymbol{\kappa}$ = 0.66. This study showed the reliability of using metal artifact reducing technologies to diagnosis evaluate ALVAL in patients who have undergone MoM HA. The limitation observed was in differentiating mild MoM diseases from infection.

1.2.2 Metallosis

Metallosis is a medical condition defined by a buildup of metal debris in soft tissue. In relation to THA metallosis is caused by abrasive wear around the prosthesis, not corrosion [11]. In can be generated by friction between an articulating surface and a non-articulating surface, or between two articulating surface [12]. Metallosis around the acetabular component can be caused by wear through of the liner, fracture, or dislodgement of the polyethylene insert [13-15]. This will lead to the femoral head having direct contact with the acetabular component, leading to dislodgement of metal debris from either component. Metallosis can also occur around the femoral stem, this can take place if the stem is loosened and the rough surface of the stem is subjected friction. Through fracture larger metal volumes can be dislodged from the stem. Metal ions in the joint space can lead to development of metallosis through patient hypersensitivity to the metal, or metal-ion toxicity [16].

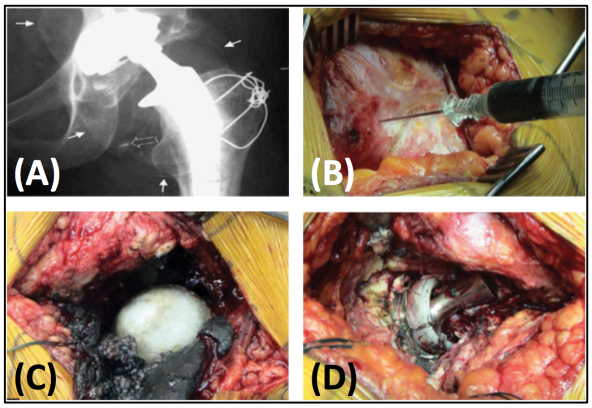

Figure 5. A: X-ray of a patient that displays radiography 'bubble sign.' Closed arrows point to the effective joint space, outlined by metallic debris. Open arrow points to broken tine. **B:** Black fluid aspirated from hip joint. **C:** Black fluid fills joint space, staining periprosthetic tissue; also a dislodged polyethylene liner. **D:** Damage to both acetabular component and the liner; also excessive metallic debris. [11]

There are no specific symptoms of metallosis compared to other conditions that lead to THA failure. There are several indicators of metallosis that can be seen in traditional radiographs. Dislodgement or significant wear may be indicative of metallosis, typically exhibited by an eccentrically positioned femoral head. Can also be diagnosed through radiographs if there is a curved region of radiolucency under the femoral neck, metal debris may present in this region as well as a radiographic bubble [11]. If metallosis is present in the patient, there will be a dark gray/black synovial fluid yielded by aspirating the patients hip joint. Metallosis can be detected in MRI through presence of synovitis and low signal presentation of the metal debris. To treat metallosis the metal debris will be removed around the joint, bone graphs will be ordered if osteolysis has occurred, and the components of the prosthesis will be replaced as needed [11].

1.2.3 Pseudotumors

Davis et al. defined pseudotumors as a non-neoplastic and non-infectious cystic or solid mass associated with a HA. Pseudotumors are seen in 1-39% of all THA cases, however 58-78% of cases are asymptomatic [17]. Patients may complain about groin pain, hip discomfort, paresthesia (pins and needles sensation), display an abnormal gait or a noticeable mass near the implant. Pseudotumors are often linked to adverse reactions to metal ions. While most common in patients who have undergone a MoM THA, pseudotumors can still occur with metal on polyethylene and ceramic on polyethylene THA prosthesis [17]. Common factors for shedding that leads to pseudotumors are poor fit of the components, mismatched metal alloys, and high frictional torque.

A physician will order an x-ray for patients exhibiting symptoms related to pseudotumors or other ALTR conditions. Anteroposterior and lateral radiographs will typically be requested; however these images have a poor sensitivity for detection of pseudotumors [18]. CT can also be done for evaluation of osteolysis, bones, hardware, periprosthetic fracture, and metallosis. Like MRI, there are complications of using CT around metal implants, specifically beam hardening and scattering [19]. The modality is adequate in detecting occult cystic and solid pseudotumors but has less sensitivity for diagnosing ALVAL [20]. Use of iodized contrast is often used for localization and characterization of periarticular cystic pseudotumors, bursal-centered masses, and soft tissue fluid collections. Ultrasound, is an inexpensive and mobile modality, works well for initial assessment of tumors. However, due to the scans being user dependent, ultrasound is rarely used for preoperative assessment.

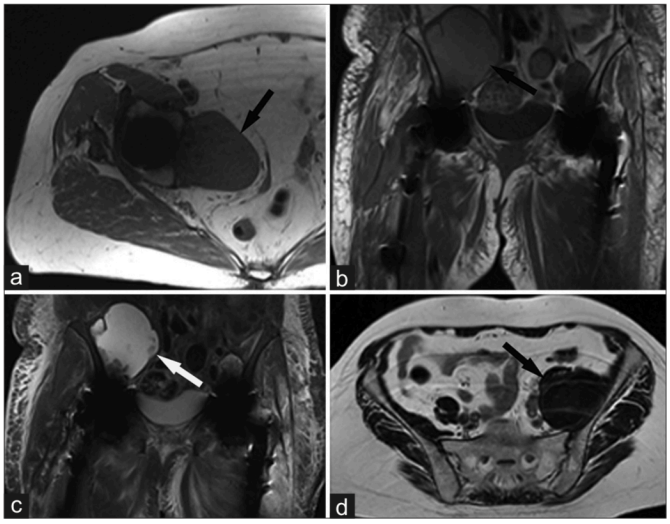

Figure 6. Three subjects exhibiting pseudotumors. **A:** 75-year-old woman, axial T_1 weighted image. 77-year-old male, **B:** T_1 weighted, **C:** short tau inversion recovery weighted. **D:** 67-year-old female, axial T_2 weighted image [17]

Pseudotumors have a variable appearance in MRI, ranging from thin walled cystic lesions to poorly defined solid masses. Often pseudotumors will be associated with synovial thickening, fluid, and debris. There exists a grading system for assessing pseudotumors in MRI images. Type 1 is defined as thin walled cystic mass (<3mm), type 2 is a thick walled cystic mass (>3mm, but less than the diameter of the cystic component), and type 3 which is thick walled and mostly a solid mass. The severity of related symptoms and revision rate has been shown to increase from type 1 through type 3 [21].

1.2.4 Osteolysis

While bone resorption is a function of normal physiology, a condition known as osteolysis exists when there is greater bone resorption (through osteoclast activity) than bone formation (osteoblast activity) [22]. There are many common mechanisms by which

osteolysis can occur following THA. Ageing is a natural source of osteolysis, women experience a loss of up to a third of their cortical bone and half of their trabecular bone mass throughout their life; bone loss is less in men, about 60% compared to women [23]. Bone is subjected to constant remodeling and stress shielding based off of the loads applied to them. When a metal implant is inserted into the hip joint it will be responsible for absorbing more of the stress, leading to less stress being applied to the surrounding bone. Since the bone is no longer subjected to high stresses, it will undergo bone resorption at an accelerated rate. Synovial pressure in the joint space as a result of ALTR can lead to osteolysis [24]; this happen through disruption of normal perfusion and oxygenation of the bone.

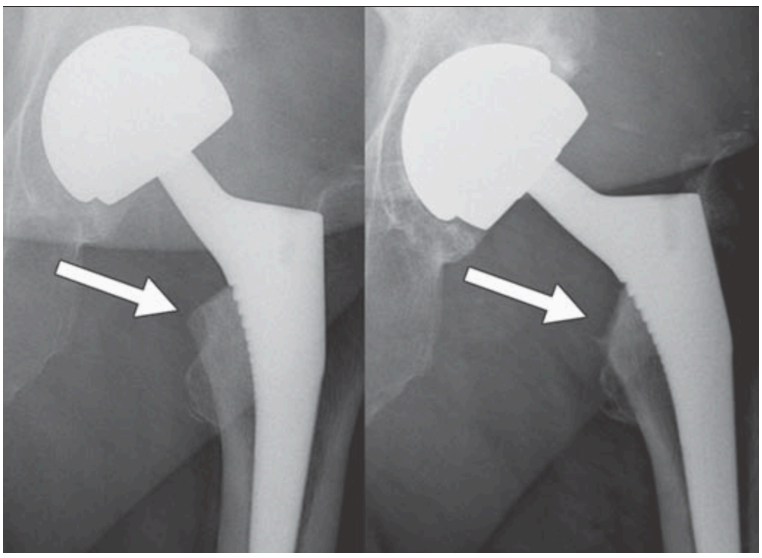

Figure 7. 64-year-old male, anteroposterior radiography at 3 months (left) and 2 years (right) after surgery, arrow demonstrating medial calcar resorption [8]

Since osteolysis is the resorption of bone, the most common modality of diagnosis is by radiographs. MRI can be used in evaluating ALTR, an underlying cause of

osteolysis, but can be unnecessary because of the ability of radiographs to assess bone loss. Surgery to combat osteolysis will be scheduled if the bone loss is extensive or progressive [25]. The two goals of this surgery are to repair the bone that has been subjected to osteolysis, and to achieve long-term stability. These goals are achieved through bone graphs. The bone graphs must result in osteogenesis, the ability to self generate new bone formations; osteoinduction, where the affected area can recruit mesenchymal stem to differentiate into new cells; and osteoconduction where the bone will have an ingrowth of capillaries and perivascular tissue [22].

1.3 Objectives of the Study

The first objective of this study was to examine three different registration techniques used together to register a THR imaged with 1.5T and 3T MRI scanners. The three techniques were a rigid body registration utilizing MATLAB's built-in functions, a least-squares fitting of 3-D point sets, and a non-rigid affine registration using MATLAB's functions. A successful registration is necessary for future work that will seek to create an atlas from a large cohort of subjects who have received a THR. This atlas will be used along with other segmentations of diseased periprosthetic tissue to create probability mapping of diseased tissue around the hip to aid physicians in diagnosis of ALTR.

The second objective was to examine the difference in the size of the metal artifacts when imaged at 1.5T vs. 3T. As field strength increases, so does the size of the artifact caused by the prosthetic. The percent difference between the artifact size at 1.5T vs. 3T was calculated. This is an important examination due to increased presence of 3T

scanners clinically, and their availability. The size of the artifact is important for future studies examining the periprosthetic tissue.

2 Methods

2.1 MRI Susceptibility and MAVRIC

Magnetic susceptibility is a measure of the extent that a substance becomes magnetized when placed in an external magnetic field [26]. Diamagnetic materials disperse the main field; whereas paramagnetic, superparamagnetic, and ferromagnetic materials concentrate the field. Two common metals used for THA are titanium and cobalt-chromium. Titanium is paramagnetic, meaning it is weakly magnetized by an external field [27]. While cobalt is ferromagnetic [27], the cobalt-chromium alloy used in prosthetics is non-ferromagnetic [28], making it safe for MRI. When imaging metal implants with MRI there is a signal void, compared to x-ray where there will be a bright representation to indicate the prosthetic. The metal implants can cause sever variations of the magnetic field as result of the susceptibility differences between the soft tissue and the metal [29]. The variations in the magnetic field, if severe enough, can lead to frequency variations in the readout and slice selection. Since the frequency varies spatially the resulting image can have signal shifted away from its original region, this will lead to signal ‘pile-up’ or loss of signal [29].

This study will be implementing GE’s multi-acquisition variable resonance image combination (MAVRIC) technology. MAVRIC corrects both in plane and through-slice artifacts common in MRI. One key feature of MAVRIC is that it uses frequency-selective excitation instead of exciting a slice or slab [29]. This acts to limit the range of frequency offsets imaged at a time. Slice direction distortion is reduced by using phase encoding to resolve in this direction. To image in 3D, acquisitions are repeated for a range of

frequencies and the final image is calculated using a sum of squares of these acquisitions. The resulting image exhibits artifact reduction as well as signal from a wide range of frequency offsets near the metal prosthetic [29]. This study will be using MAVRIC selective (MAVRIC SL) acquisition, which has been shown to significantly reduce artifacts compared to 2D FSE when imaged at a 3T field strength [30].

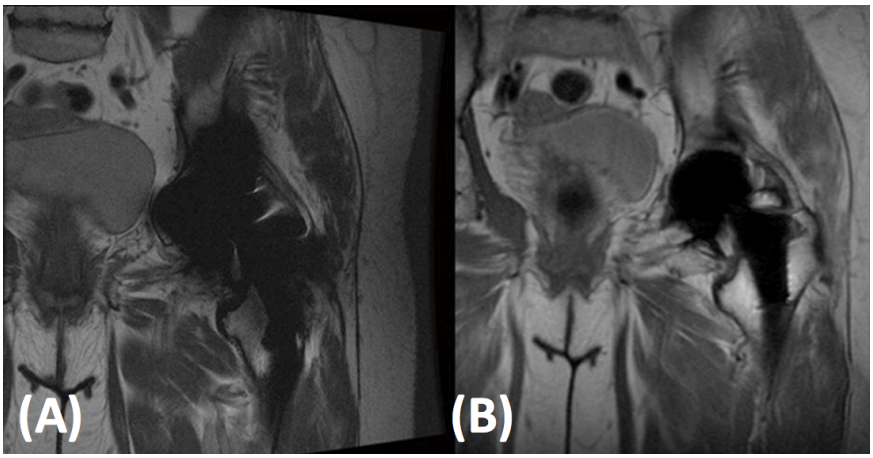

Figure 8. Artifact reduction capabilities of MAVRIC SL (**B**) compared to 2D FSE (**A**) [31]

2.2 Rescanning of Subjects

30 subjects who were previously imaged with 1.5T GE scanners, using MAVRIC SL software, were recruited for this study. They were imaged with GE's Discovery MR750 3T MRI using MAVRIC SL. For the 3T images the dimensions were 512x512 with 32 slices, field of view of 400mm, slice thickness of 4mm, and an echo time of 6.528ms. Since the 1.5T images were not acquired as a part of a single study there was some variability of the imaging parameters. The field of view was between 380 and

480mm, number of slices between 24 and 40, and an echo time ranging from 6.352 and 6.848ms.

2.3 Registration of 3T Hip Prosthesis to 1.5T Prosthesis

Once the data sets were acquired from all subjects, the next step was to register the prosthetics imaged with a field strength of 3T to those imaged at 1.5T. First the acetabular components were registered together, then the femoral components, finally they were combined and a non rigid registration was performed. The two components of the THA were separate rigid bodies, therefore they had to be registered independently.

2.3.1 Registration of the Acetabular Components

The registration of the acetabular component was performed using MATLAB's built in "imregister" function. This registration tool allows for the user to register two volumes together using a translation, rigid, similarity, or affine transformation [32]. For this step a rigid transformation was used to preserve the shape and size of the prosthetic. Initially, it was attempted to register the acetabular components to each other. This was unsuccessful due to the mismatch in the size of the prosthetic when imaged at two difference field strengths. The signal void indicating the metal prosthetic was larger in the 3T images than in 1.5T. This aligns with the principle of the susceptibility artifact size equation, that states that an increase in field strength will result in greater susceptibility artifact size. It was concluded that the best way to register two artifacts would be to first determine the registration transform for a bone fixed to the acetabular component, then apply it to the acetabular volume. The ilium proved to be an easy bone to trace, and was

also attached directly to the acetabular component. One last step had to be taken before the registration could be calculated. An initial translation registration was performed in order to align the centers of mass of the two volumes. The built in registration tool would often calculate large angle transformations if this was not done, the moving volumes would sometimes be rotated 45º in the coronal plane. The geometric transformation calculated by the registration was then applied to both the acetabular component and the ilium.

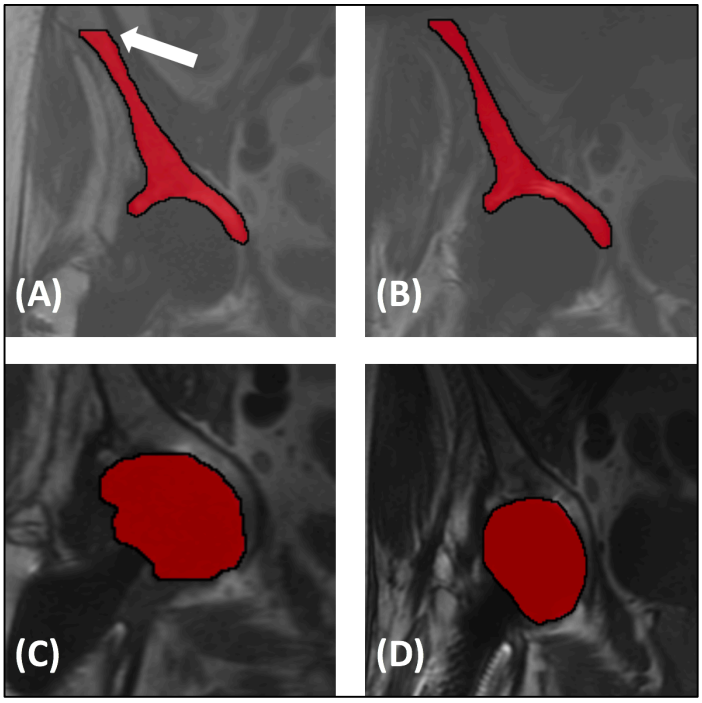

Figure 9. First row has the tracings of ilium from 1.5T (**A**) images and 3T (**B**). The arrow points to where the ilium from 1.5T images had to be cut off due to the entire ilium not being captured at 3T. The second row contains tracings of acetabular component from 1.5T (**C**) images and 3T (**D**).

The ilium in the 1.5T and 3T images were traced side by side using Horos, a DICOM viewer. This was done because the center of the field of view from the 1.5T

images can be inferior or superior to 3T images. This can result in part of the ilium not being imaged. The ilium also was not fully captured in either the anterior or posterior direction. Tracing them together allowed for only volume in present in both images to be traced. There were subjects that images could not be used for in this study, either because too much of the superior ilium was not captured, or because significant artifacts throughout the ilium inhibited tracing. In figure 10 the subject had metal hardware throughout the ilium, suspected to be a plate to correct an issue with the pelvis.

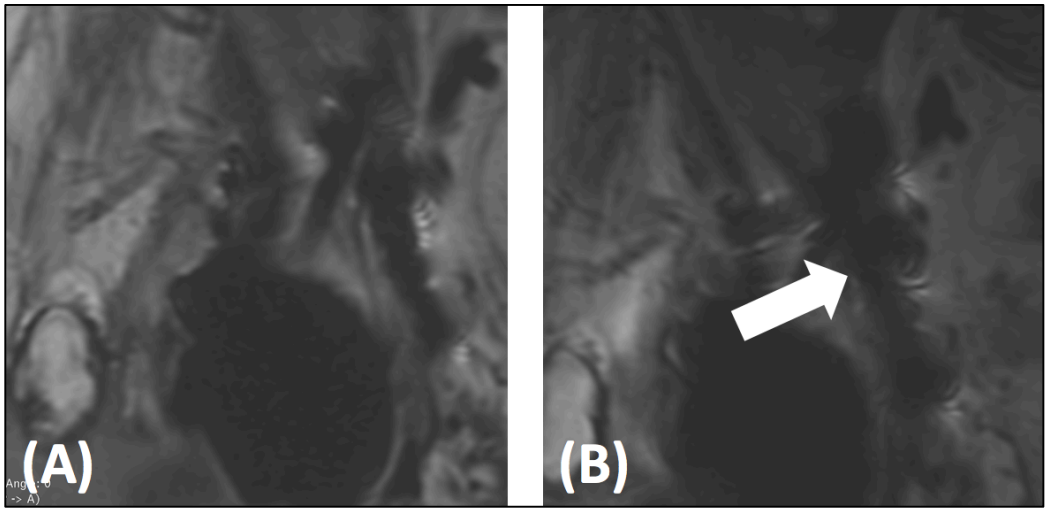

Figure 10. An instance where additional artifact not from the acetabular component was severe enough to inhibit tracing of the ilium at both 1.5T (**A**) and 3T (**B**).

Before the hips were registered, the size of the volume of both 3T and 1.5T artifact was determined. It was expected that the 3T volume would be greater than the 1.5T volume. The increase of the 3T artifact was determined by subtracting the 1.5T volume from the 3T volume, then dividing by the 1.5T volume. It was determined how

well the ilium registered by determining how much of the 1.5T volume intersected with the 3T volume. The same error analysis was performed for the acetabular components.

2.3.2 Registration of Femoral Components

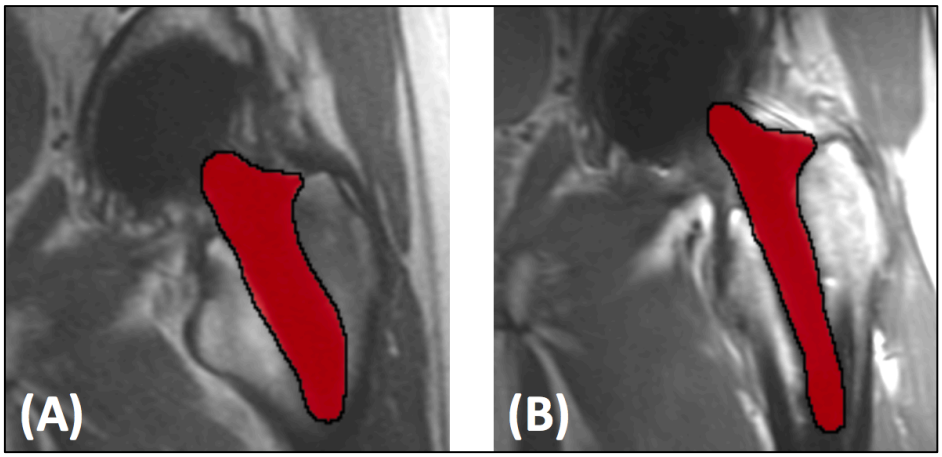

Figure 11. The tracings of the femoral component imaged at 1.5T (**A**) and 3T (**B**)

Next the femoral component was traced (figure 11) from both data sets. Initially the method of registering bones fixed to the component was implemented. This failed because too much of the connected bone (the trochanter) was lost due to the metal artifact, resulting in poor registration of the femoral component. Instead a method of transforming three anatomical markers from the 3T images to the 1.5T images was implemented. The transformation of these three points (rotational and translation) was calculated with equation below [33,34].

$$P_{1.5} = R * P_3 + t$$

R and T are the rotational and translational transformation matrices respectively; and the two P variables are the datasets containing the x, y, and z geometric coordinates of the three anatomical markers. The anatomical markers had to be recorded in Horos. The three points were the lesser trochanter, greater trochanter, and the most distal point of the implant located midway down the femur.

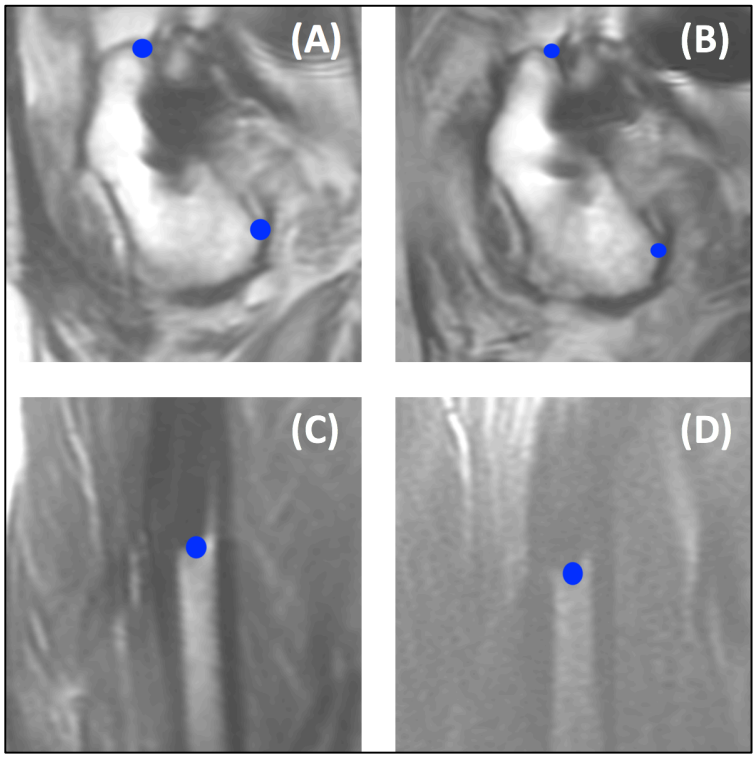

Figure 12. The first row has landmarks of the greater (top) and lesser (bottom) trochanter at 1.5T (**A**) and 3T (**B**). The second row has the end of the femoral stem component landmarked at 1.5T (**C**) and 3T (**D**)

There were soft tissues that aid in consistent marking between the two image sets. The iliotibial band and deep trochanter bursa were used to help mark the greater trochanter, the iliopsoas tendon aided in marking the lesser trochanter. There was consistency throughout the subjects where the left lesser trochanter was not visible in the

3T images. When this happened the iliopsoas tendon was essential for determining the landmarks location (figure 13).

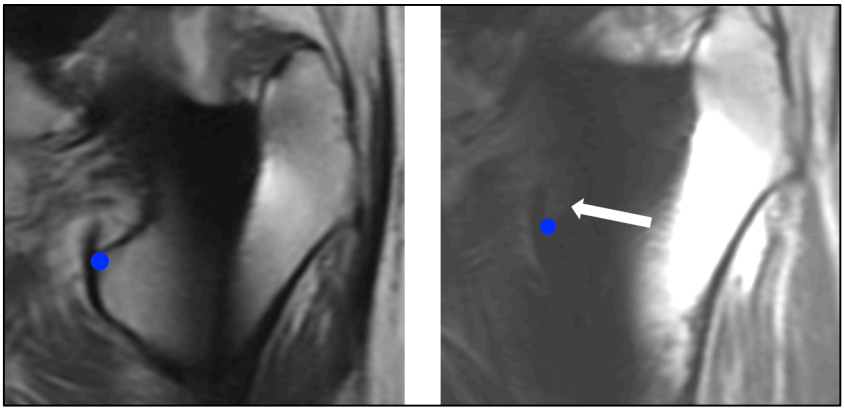

Figure 13. An instance where the greater trochanter was not visible at 3T (right) compared to at 1.5T (left). The iliopsoas tendon (marked with the arrow) was used to landmark the lesser trochanter at the same point between the 1.5T and 3T images

Once all of the anatomical markers were recorded, the rotational and translation transformations were calculated using a least-squares fitting of 3-D point sets [33], implementing a MATLAB algorithm written by Nghia Ho [34].

$$centroid = \frac{1}{N}\sum_{i=1}^{N} P^i$$

The first step was to calculate the centroid of each set of three points.

$$H = \sum_{i=1}^{N} (P_3^i - centroid_3)(P_{1.5}^i - centroid_{1.5})^T$$

Second step was to determine the familiar covariance matrix of the two sets, which includes centering both sets so their new centroids are at the origin.

$$[U, S, V] = SVD(H);\ \ where\ H = USV^T$$

$$R = VU^T$$

To determine the rotational matrix a singular value decomposition was performed on the familiar covariance matrix. U and V are 3x3 orthonormal matrices [33], where their columns made up of the left and right singular vectors.

$$t = -R * centroid_3 + centroid_{1.5}$$

Lastly the translation component was determined by finding the difference between the rotated 3T centroid and 1.5T centroid. The rotational and translation transformations were then applied to each point of the 3T femoral component mask. This was done by calculating the geometric location of each point of the mask and then applying the transforms. The percent alignment and difference in artifact size were calculated in the same way as was done for the ilium and acetabular component.

This registration method was validated by performing the same registration technique on the native hips of three subjects. The trabecular bone was traced using Horos and the locations of three landmarks were recorded. The greater and lesser trochanter were again used; but since there was no implant, a new landmark had to be chosen to replace the “end of the femoral stem component” location. A location on the

femoral head was chosen that exhibited a distinguishable feature (such as an indentation) in both the 1.5T and 3T images. This method was validated by determining the percent alignment.

2.3.3 Registration of All Components

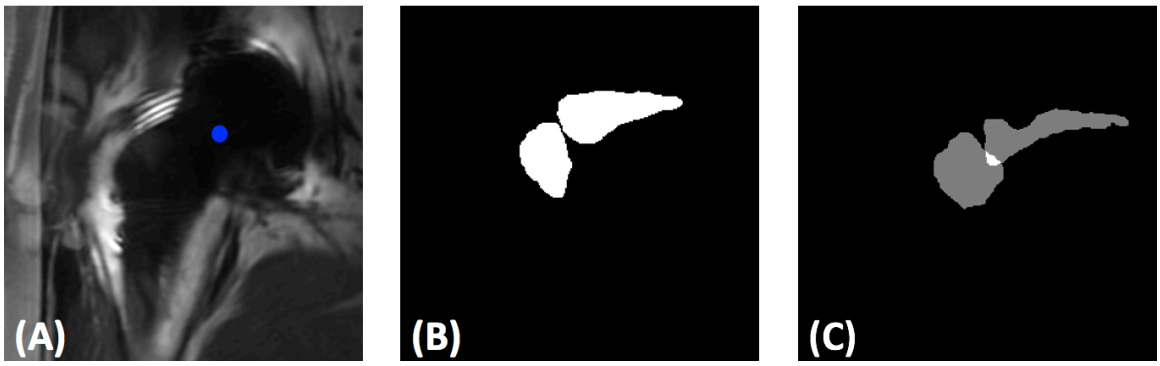

Figure 14. The first image is the common point where the acetabular and femoral component intersect (**A**). The last two images are of the two components before (**B**) and after (**C**) the stem was shift so the common point was in the same position for both components.

Finally, the two components from the 3T images were combine and registered, using a non-rigid transformation, to the 1.5T total implant. A common point between the two volumes was recorded (figure 14. A). The stem was translated so that the common point would be at the same location on the acetabular and femoral component in the combined image. Where there was overlap between the two components, the signal from the acetabular component was chosen to populate the volume. The "imregister" function was applied to find the affine transformation (comprised of rotation, translation, resizing, and shear components). The transformation was then applied to the 3T volume. To examine the soft tissue surrounding the implant a 3D dilation was applied to the mask of

the image that would dilate the volume by 1cm. A function to create the structuring element for the dilation was developed in MATLAB, this function accounted for differences between the in-plane resolution and slice thickness for the 3D structuring element.

3. Results

3.1 Acetabular Registration Results

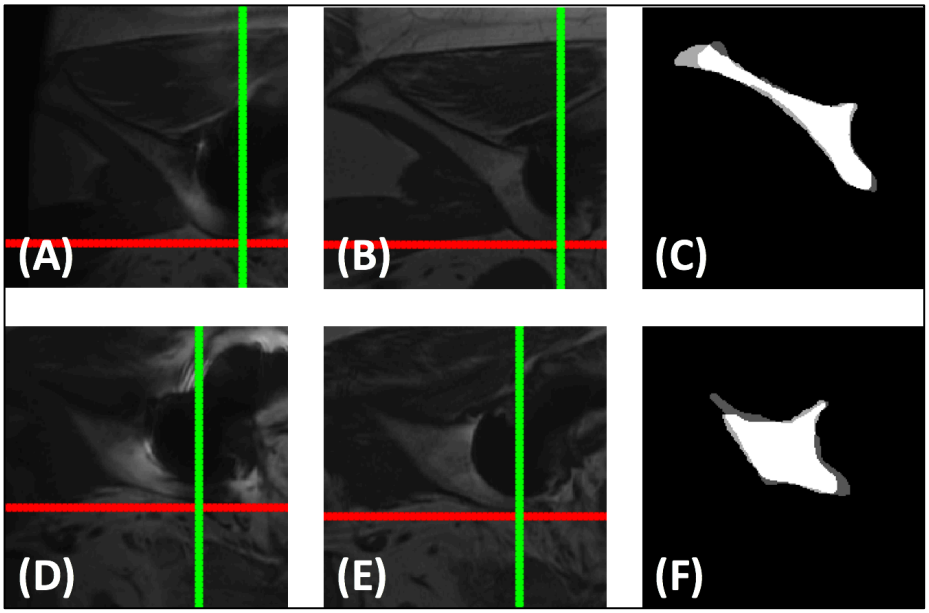

Figure 15. The first column has the registered 3T images, second column contains the 1.5T images, and the last column has the two masks registered together (white is overlap, dark gray is unmatched 3T mask, light gray is unmatched 1.5T mask)

A: 3T DICOM volume registered to the volume from the 1.5T Volume (**B**). **D** (3T) and **E** (1.5T) are the registrations from another slice from the same subject. **C** and **F** are the registration of the ilium mask where white is the intersections 1.5T and 3T, light gray is the non-intersecting 1.5T volume, and dark gray is the non-intersecting 3T volume. It was noted that the curvature lining the acetabular component had consistently been aligned between the 1.5T and 3T volume. This may be due to this region being fully captured by the scans across all subjects since imaging the entire hip prosthesis was the

primary goal of each of the scans. This proved to be advantageous when the transforms were then applied to the acetabular tracings.

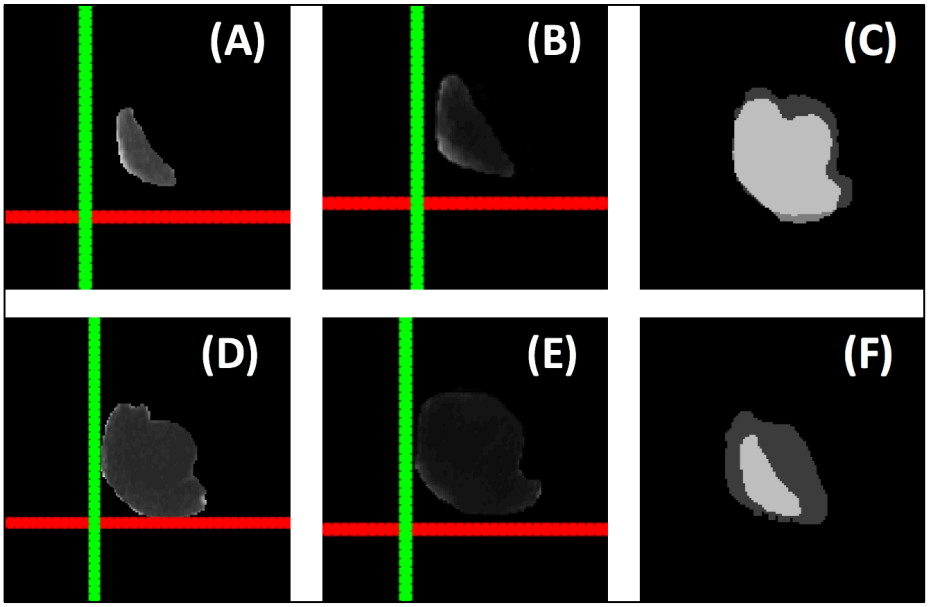

Figure 16. The first column of this figure has the registered 3T images, second column contains the 1.5T images, last column has the two masks registered together (white is overlap, dark gray is unmatched 3T mask, light gray is unmatched 1.5T mask)

A (1.5T) and **B** (3T) show the calculated ilium registrations applied to the volume tracings of the 3T acetabular component compared to the 1.5T volume. **D** (1.5T) and **E** (3T) are the registrations from another slice in the same subject. **C** and **F** are the registration of the acetabular masks, where white is the intersections of 1.5T and 3T volumes, light gray is the non-intersecting 1.5T volume, and dark gray is the non-intersecting 3T volume. The registrations between the two acetabular components worked successfully as exhibited in figure 16. It is seen that the area peripheral to the ilium in image A was lined up for both volumes. The increase in metal susceptibility

artifact when imaging at 3T compared to a 1.5T field strength is seen in both the volumetric images and the masks.

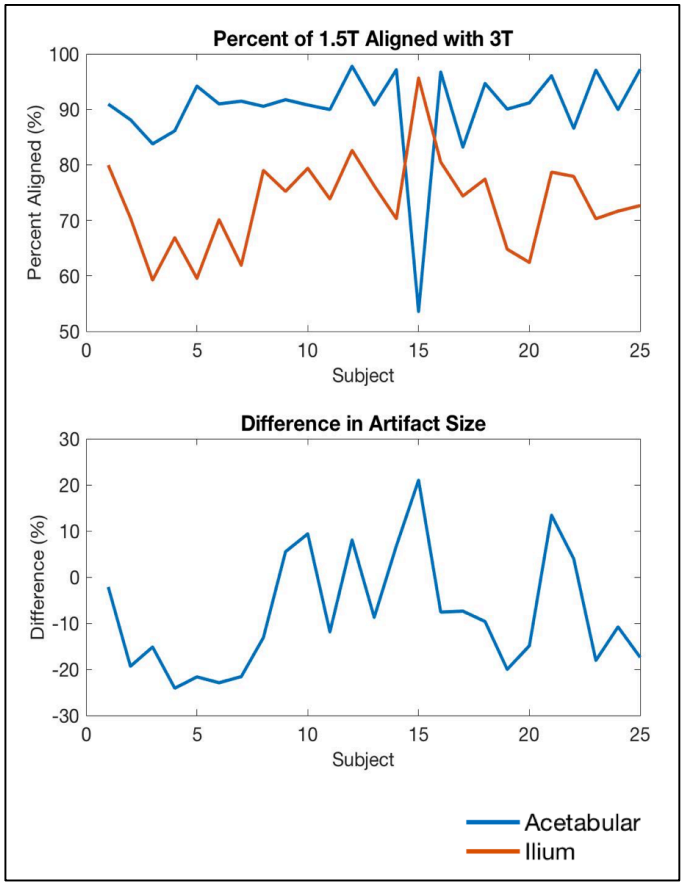

Figure 17. The first graph of plots the percent of the 1.5T mask that aligns with the 3T mask after registration of the ilium and acetabular component. The second graph plots the difference in artifact size between the 3T and 1.5T masks.

Segment Registered	Percent of Volume Aligned (%)	Difference in Artifact Size (%)
Ilium	73.24 ± 8.22	
Acetabular	90.03 ± 8.64 (S,T)	-7.93 ± 12.75 *
Femoral Stem	67.89 ± 14.74 (A,T)	−5.49 ± 19.29
Total	77.64 ± 12.64 (A,S)	

Table 1. An **A**, **S**, or **T** indicates a significant difference in the percent alignment between the registration and the registration performed for the acetabular, femoral component, or total implant respectively. A (*) indicates a significant statistical difference between the sizes of the 1.5T and 3T artifact volumes.

With the exception of subject 15, the volumes of the 1.5T volumes aligned successfully to the 3T volumes for the acetabular component (mean = 90.03%, SD = 8.64%). The volumes of the ilium were not as well aligned (mean = 73.24%, SD = 8.22%), this can be in part attributed to the volumes only being partially imaged. A two tailed t-test was also performed on the data with a p-value of 0.05. If the error metric from one registration had a value significantly different than the same metric for a different registration it was marked with an A, S, or T to indicate significance from the acetabular, stem, or total registration errors respectively. The volume of the acetabular artifact was on average 7.93% less at 3T compared to 1.5T.

3.2 Femoral Registration Results

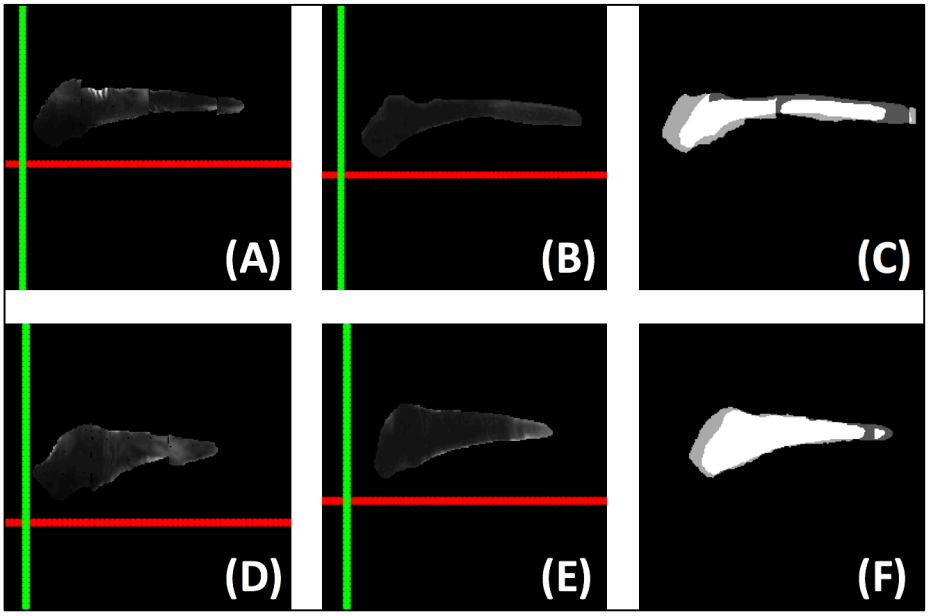

Figure 18. The first column has the registered 3T images, the second column contains the 1.5T images, and the last column has the two masks registered together (white is overlap, dark gray is unmatched 3T mask, light gray is unmatched 1.5T mask).

A (3T) and **B** (1.5T) show the calculated ilium registration applied to the 3T volume tracings of the acetabular component compared to the 1.5T volume. **D** (3T) and **E** (1.5T) are the registrations from another slice in the same subject. **C** and **F** are the registration of the acetabular masks, where white is the intersections of 1.5T and 3T, dark gray is the non-intersecting 1.5T volume, and light gray is the non-intersecting 3T volume. The transformation applied to the stems did not result in as smooth of registration as the ilium and acetabular. This is in part due to the acetabular and ilium registrations implementing a MATLAB's built in registrations that included a bicubic

interpolation. However, the end points landmarks matched up well (far right edge of **C** and **F**).

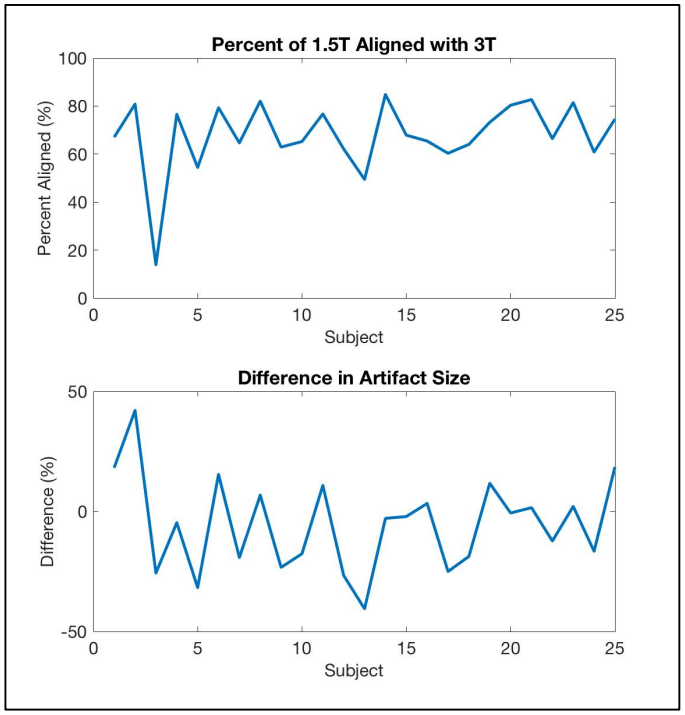

Figure 19. The first graph plots the percent of the 1.5T mask that aligns with the 3T mask after registration of the femoral component, and the second graph plots the difference in artifact size between the 1.5T and 3T masks.

The average alignment of the two femoral volumes was lower and more varying (mean = 67.89%, SD = 14.74) with this registration than for the acetabular registration. The volume of the femoral component artifact was on average 5.49% less at 3T compared to 1.5T.

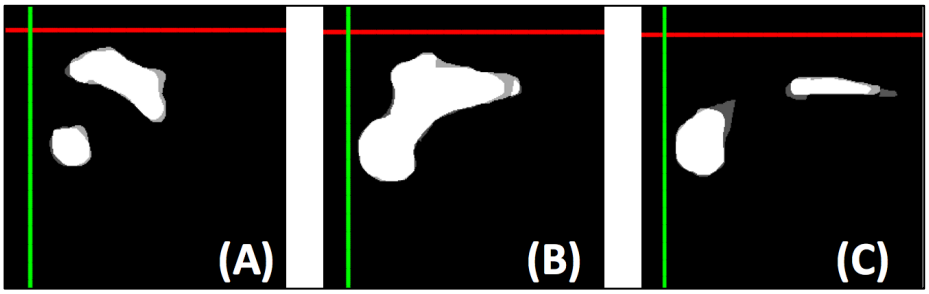

Figure 20. These three images have the combined masks where white is the overlap between the two volumes, the dark gray is the unmatched 3T volume, and light gray is the unmatched 1.5T volume.

The average percent alignment of the trabecular bone was 85.40%, greater than the alignment of femoral component's artifact. It was noted that there was more alignment near the landmarks, and less alignment around the stem of the trabecular bone.

3.3 Total Registration Results

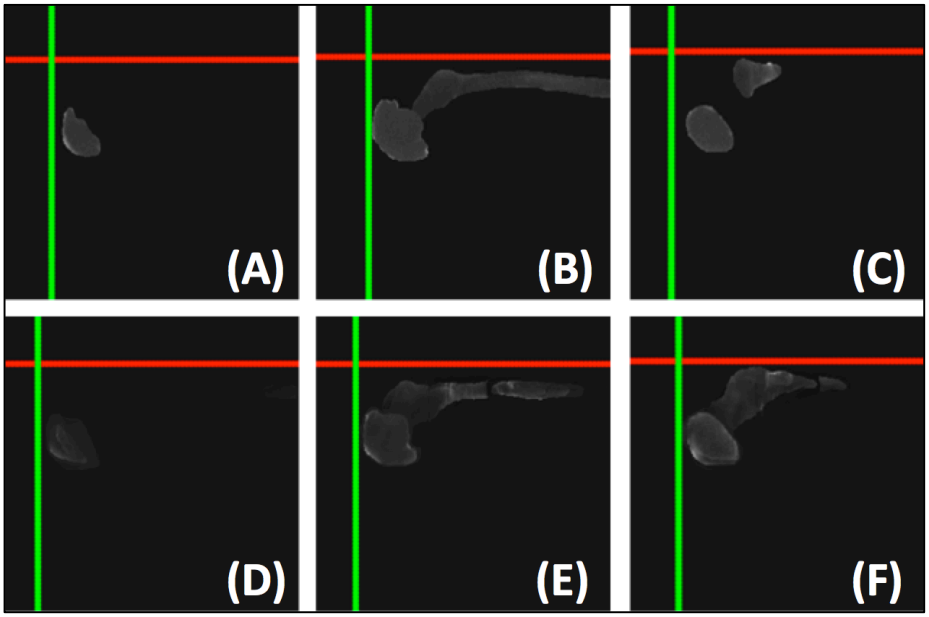

Figure 21. The top row has images from the entire implant imaged at 1.5T, and the second row consists of the corresponding slices of the registered 3T volume.

The rigidness of the femoral components is visible, same as with the independently registered stems. A slight increase in artifact size is also noted for 3T volumes, it is undetermined if this is due to increased metal artifact susceptibility at 3T or due to the transformation applied to the femoral components.

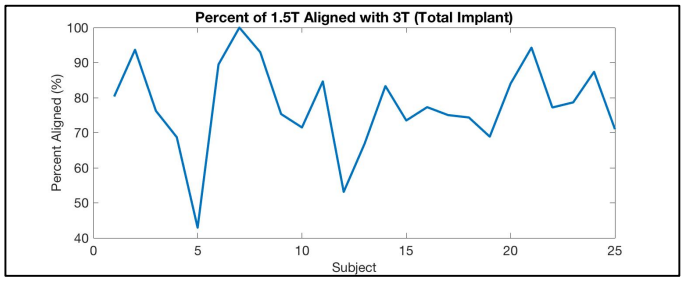

Figure 22. This graph plots the percent of the 1.5T mask that aligns with the 3T mask after registration of the entire implant.

The total registrations yielded a percent alignment between those calculated for the acetabular and femoral components (mean = 77.64%, SD = 12.64%).

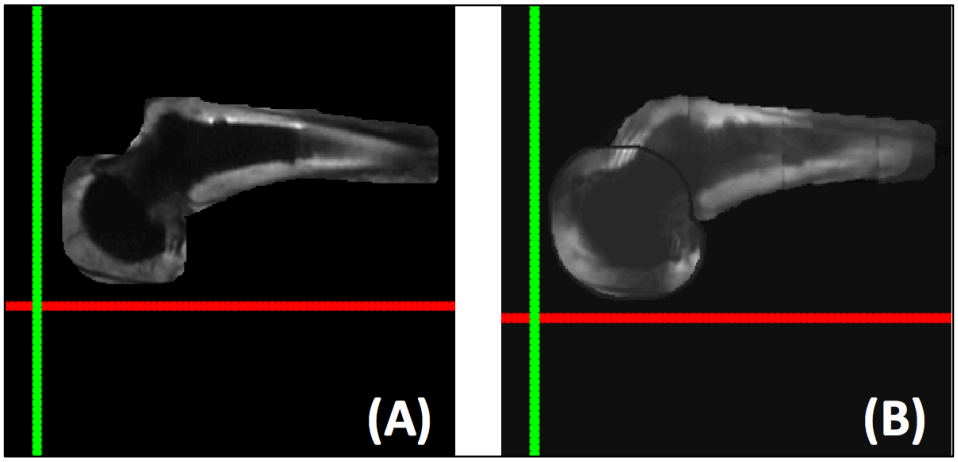

Figure 23. Image **(A)** is the 1.5T volume of the implant dilated to include 1cm of the periprosthetic tissue and connecting bone, and **(B)** is the corresponding registered 3T volume.

The volumes of the both acetabular and femoral components were both dilated to capture 1cm of peripheral tissue. The calculated registrations were then applied to each component. This operation was done to provide an example of the implications of the preceding registrations; allowing for peripheral soft tissue examination

4. Discussion

4.1 Registrations

The results of the acetabular registrations were promising. With an average 90.03% of the 1.5T volume aligning with 3T volume, the method of registering peripheral bones to one another, in this case the ilium, proved to be a viable method for registration. However, there are ways that this could be improved. One way would be to have the entire ilium imaged by centering the scan a few centimeters more superior on the body. Another possible way to improve this method would be to test registering other parts of the pelvis (i.e. ischium or pubic bone) together, and then applying the transformation to the acetabular component. There are no other comparative studies that register two signal voids to one another, so background on validating that the two volumes registered properly was limited. One possible way to further asses the two volumes registered successfully would be to implement a shape matching metric that would account for the varying size of the artifact due to the magnetic field. Another way of validation would be to analyze similarity of the peripheral tissue that isn't affected by the signal void. A possible issue of this is that the surrounding soft tissue anatomy varies with time as a result of any of the aforementioned disease states related to hip arthroplasty. The 1.5T artifact of the acetabular component was significantly greater than the 3T artifact. This result was not expected, since MR physics dictates that susceptibility artifact size increases with field strength. The best explanation for this is user error when tracing the signal void. When tracings were conducted the focus was tracing what was

clearly the implant, and not surrounding tissues that had their signal distorted due to the metal artifact.

The result of the registration of the femoral components was not successful when compared to the acetabular component. This registration started with tracing the femoral component, which was more difficult than tracing the acetabular component. While the femoral component was well defined in the 1.5T images, the 3T images had areas that were traced with more subjectivity. The trabecular bone overlapped the more distal region of the stem, breaking up the stem component into several regions in a given slice; this differed from the acetabular which was always a single region in each slice. This registration was more effective when registering the native trabecular bones together, with a percent alignment of 85.56%. The area with poorest alignment was in the stem, and aligned well near the landmarks. It was attempted to add more landmarks throughout the bone, however the current method of solving for the transformation matrices only allows for three points. In the future, another method to solve for the transformations using more landmarks should be examined. Another problem with the femoral registration was that due to time limitations a proper interpolation function couldn't be written for the transformation. There were voxels in the resulting volume that had more than one point registered to them from the pre-transformed volume. This led to voxels where there was no signal in the registered image. The registered volumes were smoothed and a threshold was applied, but the rigid shapes still remained. One possible solution to this would be to reshape the pre-registered volume so that resolutions are same in all directions, this could possibly smooth out the image since in the original volume's coronal resolution is only about 20% of the slice thickness. Another approach would be

to register two volumes, where the only non-zero values are at the locations of the anatomical markers, and utilize MATLAB's "imregister" function with built-in interpolation. The 1.5T artifact of the femoral component was greater than the 3T artifact, however a t-test determined this difference was not significant. This was not the expected result; this was attributed to tracing errors similar to the problems experienced with the acetabular component.

The total registration had a percent alignment between those calculated for the femoral and acetabular components. Due to time limitations the MATLAB registration tool had to be used. It was attempted to apply ANTs, a registration tool that has a non-linear component in the final step of registration. This non-linear registration "balloons" out the volume, and the resulting registered shape is nearly the exact same as volume it is being registered to. The long term applications of this are to create an atlas from a large cohort of subjects who have undergone THA. Other members of this lab have been segmenting out regions that are diseased with conditions associated with THA. Integrating the registrations, segmentations, and machine learning it is possible to create a network that will aid in diagnosis of these diseases. This is vital because it is not a universal skill that radiologists have to diagnosis adverse local tissue reactions from images acquired by MRI.

4.2 Future Directions

With advancements in pharmaceutics early detection of ALTR has become more important. Cytokines are a major mediator of induced adverse responses to debris, there are anti-inflammatories that can be used to modulate their release [35]. Anti-osteolytic

agents can be taken to disintegrate osteoclast's (cells that break down bone tissue) morphology. Advances in gene therapy have demonstrated the capabilities of viral vectors to deliver anti-inflammatory cytokine genes to periprosthetic tissues, limiting inflammation and extending the life of the prosthetics [22]. The United States spends about $15 billion a year on hip replacements, with revision secondary to infection costing on average $96,000 [36]. While there are ways of reconstructing bone that have undergone osteolysis, it is necessary for a method to precisely diagnosis any of the diseases associated with a THA for a targeted treatment.

5. Conclusions

While the acetabular components were successfully registered together, the femoral components were not. The registration of the acetabular component might have room for improvement by using a bone other than the ilium for registration, or by having complete imaging of the ilium as a part of the acquisition protocol moving forward. The registration of the femoral component needs to have an interpolation function as a part translation process. This registration was more successful when registering the native trabecular bone. This should be the first step in determining if the point registration is viable for registering the stems. If this still does not work other methods, such as using the same registration tool used for the acetabular components should be explored. This would require a bone fixed to the femoral stem, such as the distal femur. Once this step is cleared a registration of the total hip should be performed using ANTs, allowing for an atlas of all subjects to be acquired. There was an unexpected result with the differences in artifact size between the two field strengths. It was not expected that the metal artifact would be greater at 1.5T than 3T. This is most likely due to previously mentioned user error when tracing the two component.

Bibliography:

[1] Total Hip Replacement - OrthoInfo - AAOS [Internet]. Orthoinfo.aaos.org. 2019 [cited 8 October 2019]. Available from: https://orthoinfo.aaos.org/en/treatment/total-hip-replacement/

[2] Willert HG, Buchhorn GH, Fayyazi A, Flury R, Windler M, Köster G, Lohmann CH. Metal-on-metal bearings and hypersensitivity in patients with artificial hip joints: a clinical and histomorphological study. JBJS. 2005 Jan 1;87(1):28-36.

[3] Ollivere B, Darrah C, Barker T, Nolan J, Porteous MJ. Early clinical failure of the Birmingham metal-on-metal hip resurfacing is associated with metallosis and soft-tissue necrosis. The Journal of bone and joint surgery. British volume. 2009 Aug;91(8):1025-30.

[4] Pandit H, Glyn-Jones S, McLardy-Smith P, Gundle R, Whitwell D, Gibbons CL, Ostlere S, Athanasou N, Gill HS, Murray DW. Pseudotumours associated with metal-on-metal hip resurfacings. The Journal of bone and joint surgery. British volume. 2008 Jul;90(7):847-51.

[5] Nawabi DH, Gold S, Lyman S, Fields K, Padgett DE, Potter HG. MRI predicts ALVAL and tissue damage in metal-on-metal hip arthroplasty. Clinical Orthopaedics and Related Research®. 2014 Feb 1;472(2):471-81.

[6] Duggan PJ, Burke CJ, Saha S, Moonim M, George M, Desai A, Houghton R. Current literature and imaging techniques of aseptic lymphocyte-dominated vasculitis-associated lesions (ALVAL). Clinical radiology. 2013 Nov 1;68(11):1089-96.

[7] Donell ST, Darrah C, Nolan JF, Wimhurst J, Toms A, Barker TH, Case CP, Tucker JK. Early failure of the Ultima metal-on-metal total hip replacement in the presence of normal plain radiographs. The Journal of bone and joint surgery. British volume. 2010 Nov;92(11):1501-8.

[8] Yanny S, Cahir JG, Barker T, Wimhurst J, Nolan JF, Goodwin RW, Marshall T, Toms AP. MRI of aseptic lymphocytic vasculitis–associated lesions in metal-on-metal hip replacements. American Journal of Roentgenology. 2012 Jun;198(6):1394-402.

[9] Campbell P, Ebramzadeh E, Nelson S, Takamura K, De Smet K, Amstutz HC. Histological features of pseudotumor-like tissues from metal-on-metal hips. Clinical Orthopaedics and Related Research®. 2010 Sep 1;468(9):2321-7.

[10] Anderson H, Toms AP, Cahir JG, Goodwin RW, Wimhurst J, Nolan JF. Grading the severity of soft tissue changes associated with metal-on-metal hip replacements: reliability of an MR grading system. Skeletal radiology. 2011 Mar 1;40(3):303-7.

[11] Cipriano CA, Issack PS, Beksaç B, Della Valle AG, Sculco TP, Salvati EA. Metallosis after metal-on-polyethylene total hip arthroplasty. Am J Orthop (Belle Mead NJ). 2008 Feb;37(2):E18-25.

[12] Silva M, Heisel C, McKellop H, Schmalzried TP. Bearing surfaces. The Adult Hip. 2nd ed. Philadelphia, PA: Lippincott Williams & Wilkins. 2007;251.

[13] Engh Jr CA, Hopper RH, Engh CA, McAuley JP. Wear-through of a modular polyethylene liner: four case reports. Clinical Orthopaedics and Related Research (1976-2007). 2001 Feb 1;383:175-82.

[14] Suh KT, Chang JW, Suh YH, Yoo CI. Catastrophic progression of the disassembly of a modular acetabular component. The Journal of arthroplasty. 1998 Dec 1;13(8):950-2.

[15] Brien WW, Salvati EA, Wright TM, Nelson CL, Hungerford DS, Gilliam DL. Dissociation of acetabular components after total hip arthroplasty. Report of four cases. JBJS. 1990 Dec 1;72(10):1548-50.

[16] Haynes DR, Rogers SD, Hay S, Pearcy MJ, Howie DW. The differences in toxicity and release of bone-resorbing mediators. J Bone Joint Surg Am. 1993;75:825-34.

[17] Davis DL, Morrison JJ. Hip arthroplasty pseudotumors: pathogenesis, imaging, and clinical decision making. Journal of clinical imaging science. 2016;6.

[18] Van der Weegen W, Sijbesma T, Hoekstra HJ, Brakel K, Pilot P, Nelissen RG. Treatment of pseudotumors after metal-on-metal hip resurfacing based on magnetic resonance imaging, metal ion levels and symptoms. The Journal of arthroplasty. 2014 Feb 1;29(2):416-21.

[19] Boas FE, Fleischmann D. CT artifacts: causes and reduction techniques. Imaging in Medicine. 2012 Apr 2;4(2):229-40.

[20] Fritz J, Lurie B, Miller TT, Potter HG. MR imaging of hip arthroplasty implants. Radiographics. 2014 Jul 14;34(4):E106-32.

[21] Hauptfleisch J, Pandit H, Grammatopoulos G, Gill HS, Murray DW, Ostlere S. A MRI classification of periprosthetic soft tissue masses (pseudotumours) associated with metal-on-metal resurfacing hip arthroplasty. Skeletal radiology. 2012 Feb 1;41(2):149-55.

[22] Dattani R. Femoral osteolysis following total hip replacement. Postgraduate medical journal. 2007 May 1;83(979):312-6.

[23] Rubash HE, Sinha RK, Shanbhag AS, Kim SY. Pathogenesis of bone loss after total hip arthroplasty. Orthopedic Clinics of North America. 1998 Apr 1;29(2):173-86.

[24] Aspenberg P, van der Vis H. Fluid pressure may cause periprosthetic osteolysis: particles are not the only thing. Acta Orthopaedica Scandinavica. 1998 Jan 1;69(1):1-4.

[25] Stauffer RN. Ten-year follow-up study of total hip replacement. The Journal of bone and joint surgery. American volume. 1982 Sep;64(7):983-90.

[26] Susceptibility artifact [Internet]. Questions and Answers in MRI. 2019 [cited 8 October 2019]. Available from: http://mriquestions.com/susceptibility-artifact.html

[27] Kim YH, Choi M, Kim JW. Are titanium implants actually safe for magnetic resonance imaging examinations?. Archives of plastic surgery. 2019 Jan;46(1):96.

[28] MRI Safety Information [Internet]. Zimmerbiomet.com. 2019 [cited 9 October 2019]. Available from: https://www.zimmerbiomet.com/medical-professionals/support/mri.html

[29] Hargreaves BA, Worters PW, Pauly KB, Pauly JM, Koch KM, Gold GE. Metal-induced artifacts in MRI. American Journal of Roentgenology. 2011 Sep;197(3):547-55.

[30] Choi SJ, Koch KM, Hargreaves BA, Stevens KJ, Gold GE. Metal artifact reduction with MAVRIC SL at 3-T MRI in patients with hip arthroplasty. American Journal of Roentgenology. 2015 Jan;204(1):140-7.

[31] MAVRIC SL [Internet]. Gehealthcare.com. 2019 [cited 9 October 2019]. Available from: https://www.gehealthcare.com/products/magnetic-resonance-imaging/mr-applications/mavric-sl

[32] Register Multimodal 3-D Medical Images- MATLAB & Simulink Example [Internet]. Mathworks.com. 2019 [cited 9 October 2019]. Available from: https://www.mathworks.com/help/images/registering-multimodal-3-d-medical-images.html

[33] Arun KS, Huang TS, Blostein SD. Least-squares fitting of two 3-D point sets. IEEE Transactions on pattern analysis and machine intelligence. 1987 Sep(5):698-700.

[34] Ho N. Finding optimal rotation and translation between corresponding 3D points | Nghia Ho [Internet]. Nghiaho.com. 2019 [cited 9 October 2019]. Available from: http://nghiaho.com/?page_id=671

[35] Bitar D, Parvizi J. Biological response to prosthetic debris. World journal of orthopedics. 2015 Mar 18;6(2):172.

[36] Lavernia CJ, Hernandez VH, Rossi MD. Payment analysis of total hip replacement. Current Opinion in Orthopaedics. 2007 Feb 1;18(1):23-7.